Core structure of a dissociated easy-glide dislocation in copper investigated by molecular dynamics

J. Huang

Section de Recherches de Métallurgie Physique, Centre d'Etudes Nucléaires de Saclay, 91191 Gif-sur-Yvette CEDEX, France

M. Meyer

Laboratoire de Physique des Matériaux, Centre National de la Recherche Scientifique, 92125 Meudon Principal CEDEX, France

V. Pontikis*

Section de Recherches de Métallurgie Physique, Centre d'Etudes Nucléaires de Saclay, 91191 Gif-sur-Yvette CEDEX, France

The atomic structure in the core of two Schockley partial dislocations in copper, resulting from the dissociation of a perfect easy-glide dislocation, and its influence on the fault ribbon, have been investigated for the first time as a function of temperature using molecular dynamics. We employed a resonant model pseudopotential adapted to copper. Our results show that at increasing temperature, the core of the partial dislocations becomes increasingly extended and invades entirely the fault ribbon, but the separation distance between the partial dislocation pairs is not altered. It follows that the structure of the fault ribbon differs significantly from that of an infinitely extended stacking fault and for this reason experimental determinations of the stacking-fault energy, based on the measure of the separation distance between partial dislocation pairs, should be considered with caution. We found that the temperature dependence of the fault ribbon energy in our model is mainly due to the elastic-modulus variation. Moreover, at high temperatures vibrational amplitudes of atoms are much larger in the core of the partial dislocations than in the bulk of the perfect crystal and the local atomic structure becomes highly disordered. Although disordered, the core structure remains solidlike up to the melting point T_m. Above T_m the liquid nucleates always in the core region, thus qualitatively indicating that the nucleation barrier therein is lower than in the bulk.

I. INTRODUCTION

Dislocation cores have been the object of numerous studies in the past which tried to handle the large, nonelastic strains existing in this region and thus to overcome obvious difficulties encountered by the elastic theory of dislocations. Although old, this subject is still active because the study of individual dislocations gives valuable information about the differences in the plastic behavior of various materials and also provides crucial data on the electrical and mass-transport properties associated with dislocations in low-defect materials such as semiconductors and minerals. Moreover, many of the properties of interest in materials science depend more strongly on the core structure than on the long-range stress and strain fields. Indeed, cross-slip processes and the role of dislocations as sources and sinks of point defects are highly dependent on the core structure.

Since the earlier studies, in which dislocations are treated as linear discontinuities in the strain and stress fields in an elastic continuum, it has been realized that such a description is inadequate in the case of dislocations in crystals.[1,2] In crystalline solids, large atomic relaxations occur in the core region, usually represented by a pipe surrounding the dislocation line the radius of which typically equals the Burgers vector length. Thus

an extended core configuration is produced, by far much more realistic than the localized dislocation.[3] Unfortunately, despite the remarkable advances made by high-resolution electron microscopy, the investigation of atomic relaxations near dislocations and grain boundaries is still a challenge and only indirect evidence exists of the relaxed core structure. Among others, a good example has been given recently by Legrand, who studied and definitely clarified the old problem dealing with the origin of different easy-glide planes observed in hexagonal-close-packed-structure metals.[4] To account for easy glide on the basal or prismatic planes in these materials, a variety of different criteria existed, all of which suffered serious exceptions. It has been demonstrated that this behavior is due to the fact that dislocation cores are preferentially extended either in the basal or in the prismatic planes, depending on the electronic structure of the considered metal. As a consequence, the type of the easiest glide plane in these materials is predicted in complete agreement with available experimental data.[4]

It is well known, from minimum-energy arguments, that in many materials perfect dislocations are dissociated into partial dislocation pairs separated by a stacking-fault ribbon. In face-centered-cubic (fcc) metals, the $\frac{1}{2}[110](\bar{1}11)$ perfect dislocation splits into two Schockley partial dislocations, $\frac{1}{6}[12\bar{1}](\bar{1}11)$ and $\frac{1}{6}[211](\bar{1}11)$, re-

spectively, separated by an enclosed intrinsic stacking fault. For materials with a very low stacking-fault energy γ the elastic theory predicts large dissociation distances r_0 and thus the fault ribbon can be assimilated with a stacking fault of quasi-infinite extension. The measure of r_0, using transmission electron microscopy, allows for experimentally determining γ.[5] However, in materials having a large stacking-fault energy, it is likely that the extended cores of the partial dislocations may seriously change the structure of the fault ribbon with respect to the perfect stacking fault, which is widely recognized as being a practically planar defect (i.e., relaxations along a direction normal to it are negligible[6]).

Although direct investigations of such effects are not available, pipe diffusion in dissociated dislocations can serve as an atomic level probe for structural studies since diffusion is intimately connected to the atomic structure. Experimental results on pipe diffusion in nickel have been obtained by Wuttig and Birnbaum which suggested that the fault ribbon may contribute to fast mass transport.[7] Balluffi and Granato criticized this interpretation by arguing that in the stacking-fault nearest-neighbor relationships are conserved and thus no reason existed either for a significant decrease in the formation energy of defects or for fast diffusion to occur along the fault ribbon.[8] In other words this criticism is based on the widely accepted assertion that stacking faults are essentially planar defects. Very recently however, the present authors used molecular-dynamics (MD) simulation to study pipe diffusion along a dissociated perfect dislocation $\frac{1}{2}[110](\bar{1}11)$ in copper.[9,10] The obtained results showed that, contrary to current assumptions, the fault ribbon as well as the pipes are preferential fast diffusion paths for both vacancies and interstitials. These results can be understood only if the structure of the fault ribbon differs significantly from that of an infinitely extended stacking fault and support the suggestion made by Wuttig and Birnbaum.[7]

In the present work MD is used to study the temperature dependence of the atomic structure of the Schockley partial dislocations resulting from the spontaneous splitting of a perfect dislocation in copper. We found that even at low temperatures, $T < 0.5T_m$, the cores of the partial dislocations are extended and partly cover the fault ribbon which is entirely invaded by them at high temperatures. In the cores the amplitudes of atomic vibrations are significantly enhanced with respect to the bulk crystal and an increasing disorder appears on increasing the temperature. Consequently, the local atomic structure exhibits some liquidlike features but no local melting has been observed up to the bulk melting point. When the system is heated above the melting temperature, melting occurs and the liquid phase nucleates in the vicinity of the dislocation cores. This qualitatively indicates that the nucleation barrier is lower in the perturbed core region than in the perfect crystal.

In Sec. II we present the model and the procedures we used for its validation as well as those which served to study the core structure. Section III displays the obtained results whereas Sec. IV is devoted to a brief discussion and some conclusive remarks.

II. MODEL AND COMPUTATIONS

A. Potential

The interatomic potential used in the present work was derived by Dagens from first principles using the pseudopotential theory.[11] A physically motivated fit of this potential to an analytical expression which reproduces the long-range Friedel oscillations has been realized by Lam et al.:[12]

$$U(r) = \{1 - \exp[-\alpha(r - r_1)^2]\} f_{\mathrm{osc}}(r) + f_c(r) + f_{\mathrm{BM}}(r) , \tag{1}$$

where

$$f_{\mathrm{osc}}(r) = \left[c_0 + \frac{c_1}{r^2}\right] \frac{1}{r^3}\cos\chi + \frac{s_1}{r^5}\sin\chi , \tag{2}$$

$$f_c(r) = \sum_{n=0}^{3} B_n \frac{\exp(-\beta r^2)}{r^{3-n}} , \tag{3}$$

$$f_{\mathrm{BM}}(r) = C \exp(-\gamma_1 r) , \tag{4}$$

$$\chi = \psi + 2k_F r , \tag{5}$$

$f_{\mathrm{BM}}(r)$ is a Born-Meyer repulsive term, and the values of parameters adapted to copper are given in Table I. Expression (1) is the most convenient for MD simulations and was used throughout this work instead of using tabulated values of the potential.

At each temperature the system density has been fixed to fit the experimental lattice parameter a,[13] and the potential has been modified according to the prescriptions given by Dagens.[14] Let a_0 be the value of the lattice constant at $T_0 = 300$ K, used for the calculation of the potential parameters listed in Table I, and $a(T) = a_0(1 + \varepsilon)$, its

TABLE I. Interaction potential parameters for copper expressed in units of (Ref. 12). a_0 represents the lattice constant value at $T_0 = 300$ K, used in the calculation of these parameters.

α	0.2
ρ_1	3
c_0	0.265
c_1	-0.252
s_1	20.85
ψ	1.429
β	0.163
B_0	16.55
B_1	-0.0033
B_2	0.0825
B_3	-0.1576
γ_1	0.74
C	0.1246
α_c	2.5
a_0	3.615

value at a temperatures $T > T_0$, then

$$f_{osc}(r,\varepsilon) = \frac{1}{(1+\varepsilon)^3} f_{osc}(r/(1+\varepsilon),0) \ , \qquad (6)$$

$$f_c(r,\varepsilon) = f_c(r,0) \ , \qquad (7)$$

$$f_{BM}(r,\varepsilon) = \frac{1}{(1+\varepsilon)^{a_e}} f_{BM}(r/(1+\varepsilon),0) \ , \qquad (8)$$

and the α_e value is given in Table I.

The necessary truncation of the potential in MD simulations, imposed by the finite size of the simulation box, may induce artifacts arising from the discontinuities thereby introduced in the atomic forces. To reduce such undesirable effects it is customary to apply a damping factor to Eq. (1) and to employ the resulting effective potential[15]

$$U_{eff}(r) = \exp(-\delta^2 r^2) U(r) \ . \qquad (9)$$

This procedure does not affect the value of computed physical quantities as is proven by comparing them with values obtained using the full potential [Eq. (1)].[12,15,16] In present work we used $\delta = 0.3a^{-1}$, where a is the lattice parameter.

B. Model validation

Various authors have shown that the pseudopotential derived by Dagens reproduces satisfactorily numerous physical properties of the real material such as phonon dispersion,[17] elastic constants[11,16] as well as formation and migration energies of point defects in copper.[12] However, these quantities have been calculated at zero temperature and therefore we cannot ascertain that the potential will also correctly account for finite temperature properties. Therefore, the temperature dependence of atomic mean-square displacements (MSD), $\langle u^2 \rangle$, has been computed and the results directly compare with available experimental data. Figure 1 displays the results obtained for a perfect, bulk crystal, containing $N = 4000$ particles, together with the experimental data by Owen et al.,[18(a)] Flinn et al.,[18(b)] and Martin et al.[19] Our results are in excellent agreement with the experimental values. Moreover, the choice of the system size ensures

that the computed MSD have already reached the thermodynamic limit value and do not therefore depend on the actual size of the simulated system.[20]

For materials of a given crystallographic structure the well-known Lindemann's empirical rule establishes that melting occurs when the amplitude of MSD reaches a critical percentage of the nearest-neighbor distance.[19,21,22] The perfect agreement between experimental and computed MSD we obtained strongly suggests that the melting temperature of the model may not be significantly different from that of real copper, $T_m \approx 1356$ K. However, a free-energy calculation is required to correctly predict the melting point of the model.

Because of the purposes of the present work the correct prediction of the energy of the intrinsic stacking fault is of crucial importance. Unfortunately, as we already have reported elsewhere,[16] a zero value is obtained for this quantity when the interactions are summed up to convergence. Such a behavior is not surprising since stacking-fault energy implies rather long-range interactions (beyond second neighbors) and the pseudopotential we used has not been derived self-consistently, thus its precision at long distances is poor. To bypass this limitation, we adopted an empirical compromise which consisted in the choice of an appropriate cutoff radius for the potential, $r_c = 2.3a$ (i.e., between the 10th and 11th neighbors), leading to values of the elastic moduli and stacking-fault energy comparable with those obtained experimentally (Table II).

C. Geometrical model and border conditions

The geometrical model we used consisted in a parallelepipedic box with sides parallel to the X:[110], Y:[$\bar{1}11$], and Z:[1$\bar{1}$2] crystallographic axes, respectively, and with periodic-boundary conditions acting along the [1$\bar{1}$2] direction. Two Schockley partials, $\frac{1}{6}[12\bar{1}](\bar{1}11)$, $\frac{1}{6}[211](\bar{1}11)$, separated by a distance D_0, are then introduced into the model by imposing to all atoms displacements, according to the prescriptions of the isotropic elastic theory of dislocations.[5] Overlapping atoms generated during this operation are removed. To eliminate unrealistic effects which will unavoidably rise if periodic-boundary conditions are also applied along the directions [110] and [$\bar{1}11$], we used instead fixed-border conditions: atoms are kept fixed in the outer atomic layers of the crystallite. The simulated system has therefore the form of a pseudoinfinite parallelpipedic slab along the direction parallel to the dislocation lines and contains an external
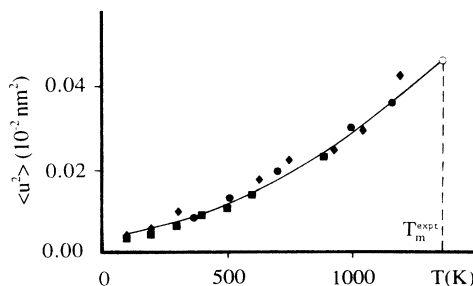

FIG. 1. Atomic mean-square displacements $\langle u^2 \rangle$ as a function of temperature. Diamonds: Perfect crystal $N = 4000$, solid squares (Ref. 18), and solid circles (Ref. 19) represent experimental values. Open circle: estimation of the value at the melting point, taken from Ref. 19.

TABLE II. Experimental and calculated values ($r_c = 2.3a$) of elastic constants and stacking-fault energy expressed in units of GPa and mJ/m^2, respectively.

	Experiment	This work
$C' = \frac{1}{2}(C_{11} - C_{12})$	25.6[a]	17
$C_{44} = C_{12}$	81.8[a]	86
γ	55.0[b]	73

[a]Reference 23.
[b]Reference 24.

static mantle surrounding the inner dynamical region where the dislocation lines are located. The thickness of the rigid lattice, d_s, has been chosen in order to avoid that atoms of the inner region feel the finiteness of the system, i.e., $d_s > r_c$, where r_c represents the cutoff radius for the interatomic forces. This procedure resulted in a system of $N_D = 7680$ dynamical particles, having lateral dimensions $4 \times ([1\bar{1}2]) \times 8$ ($[\bar{1}11]$) and containing, respectively, 81 and 79 (110) atomic planes above and below the "slip" plane. On the other hand, the static mantle contained $N_s = 4352$ particles for the cutoff radius used throughout this work, $r_c = 2.3a$, where a is the lattice constant.

D. Computations

The newtonian equations of motion were integrated by the usual central-difference algorithm[25] using a time step 0.25×10^{-14} s. This algorithm, slightly modified according to a suggestion by Bennett,[26] has also been employed to obtain a relaxed initial configuration at $T = 0$ K by quasidynamic energy minimization. To obtain equilibrium at a given temperature the system is allowed to evolve during 5000 time steps which are excluded from the calculation of the thermodynamical averages. Calculations were made at constant volume, however, at each temperature, the experimental density values[13] have been used and the potential parameters were modified as indicated above (Sec. II B).

E. Dislocation localization and analysis of the core structure

A major problem encountered when studying linear defects by MD is the localization of their position in the simulation box. A first approach consisted in computing the atomic density profile along the direction x, parallel to [110] on a local basis:

$$P(x) = \left\langle \sum_{i \in \omega} \delta(x - x_i) \right\rangle , \tag{10}$$

where the summation is made over particles pertaining to the domain defined ω by one of the atomic planes ($\bar{1}11$) immediately above or below the glide plane and large angular brackets indicate time averages. The results obtained by thermal averaging over 10^4 time steps are illustrated by Fig. 2 on which the two density profiles corresponding to these ω definitions are superimposed. The position of the two partial dislocations is clearly visible thanks to the large depression of the density profile peaks in their vicinity. The shift in the position of [1$\bar{1}$2] atomic columns above and below the glide plane, due to the local strain caused by the two partial dislocations, is responsible for this effect.

A more precise localization of the partial dislocations, which also allows the investigation of the core structure,
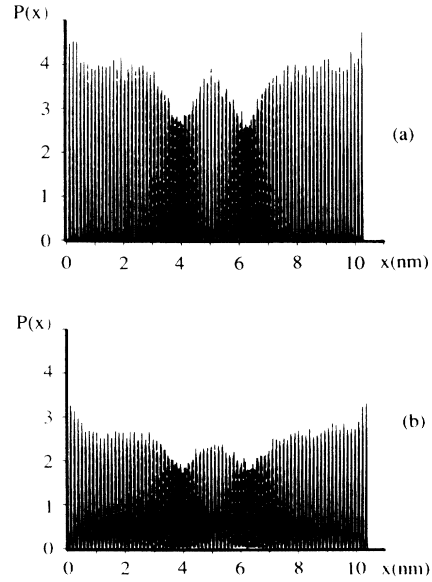

FIG. 2. Superposition of two local-density profiles above and below the glide plane along the [110] direction. Each peak corresponds to the position of atomic columns parallel to the [1$\bar{1}$2] direction (a) $T = 400$ K and (b) $T = 840$ K. The position of the Shockley partial dislocations coincides with the two depressed regions visible on this figure.

is obtained by computing the local-strain-field components ε_{xx} and ε_{yy} defined by

$$\varepsilon_{xx} = (d_x - d_{0x})/d_{0x} \tag{11}$$

and

$$\varepsilon_{yy} = (d_y - d_{0y})/d_{0y} , \tag{12}$$

where d_i and d_{0i} ($i = x,y$) represent the distances between successive peaks of average density profiles along the directions $x \parallel [110]$ and $y \parallel [\bar{1}11]$ in the defective and perfect lattices, respectively. Figure 3(a) illustrates a series of local strain profiles ε_{xx} computed at $T = 680$ K
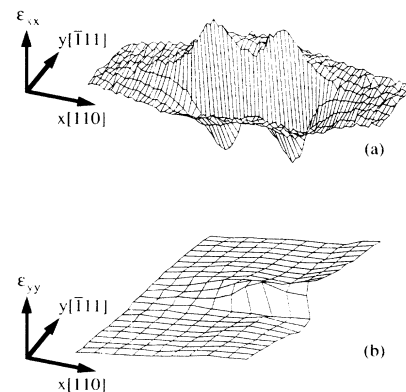

FIG. 3. Local strain profiles at $T = 680$ K, (a) ε_{xx}, (b) ε_{yy}. The perturbation is confined in the vicinity of the stacking-fault plane.

for eight $(\bar{1}11)$ atomic planes surrounding the slip plane. Using a similar representation, Fig. 3(b) represents ε_{yy} profiles each of which has been averaged over four adjacent (110) planes. Data on both figures correspond to thermal averages over 10^4 time steps. The maximum values reached by ε_{xx} and ε_{yy} are 5% and <2%, respectively. Clearly,the anelastic deformation is concentrated in the core of the partial dislocations and mainly affects the two $(\bar{1}11)$ planes adjacent to the glide plane. For the sake of simplicity we therefore consider in the following the dislocation cores to be planar defects entirely contained between these two planes. In this framework and according to the linear elasticity theory, the deformations in the core of the partial dislocations can be described by a density distribution of Burgers vectors, $\rho_x(x)$, defined by (see the Appendix)

$$\rho_x(x)=[d^l(x)-d^h(x)]/d_0 , \tag{13}$$

where $d^l(x)$, represent the local average spacing of $[1\bar{1}2]$ atomic columns pertaining to the two $(\bar{1}11)$ planes just above $(i=h)$ and below $(i=l)$ the glide plane and d_0, the ideal perfect lattice value. A similar expression can be obtained for $\rho_z(x)$. Figure 4 illustrates the profiles of the edge and screw compounds of the dislocation density distribution obtained at low, $T=107$ K and high, $T=1309$ K, temperatures. The position of the partial dislocations is identified by locating the position of the maxima on these graphs.

At increasing temperature the profiles are affected by an increase in amplitude statistical noise and the localization of the partial dislocations becomes more difficult. We therefore systematically fitted the $\rho_x(x)$ profiles on two shifted Gaussian distributions which help in determining the position and the separation between the partial dislocations.[27]

A more global representation of the core structure is finally obtained by computing both the structure-factor component with a wave vector $\mathbf{k}=(2\pi/a)[\bar{1}11]$ and the radial distribution function $g(r)$ on a local basis.[28] The domain ω used for this local analysis is a cylinder surrounding each partial dislocation whose radius R_ω equals the half-width of the above shown dislocation density distributions (Fig. 4).

F. System setup at a given temperature and border conditions

Since fixed-order conditions are used along the [110] and $[\bar{1}11]$ directions, the preparation of the initial configuration at each temperature needs careful preparation in order to avoid undesirable mismatches between the static and the dynamical parts of the system. Thus, the equilibrium separation between the two partial dislocations was determined by a MD procedure, similar in spirit to that suggested by Perrin et al.[29] for static calculations and is illustrated by Fig. 5. The initial separation, D_0, of the partial dislocations was first chosen using the elasticity theory[5] and the value of the stacking-fault energy, $\gamma=73$ mJ m^{-2}, corresponding to the cutoff radius value.[16] Relaxations in the inner region of the model at a given temperature lead to new positions for the partial

dislocations now separated by a distance D_1. These relaxations enhance mismatches between the static and the dynamical parts of the system which should be minimized by iterating the aforementioned procedure, i.e., by ascribing new positions to the atoms pertaining to the static and dynamical parts of the system, using as input the value of the separation distance D_1. The equations of motion are then integrated for a number of time steps
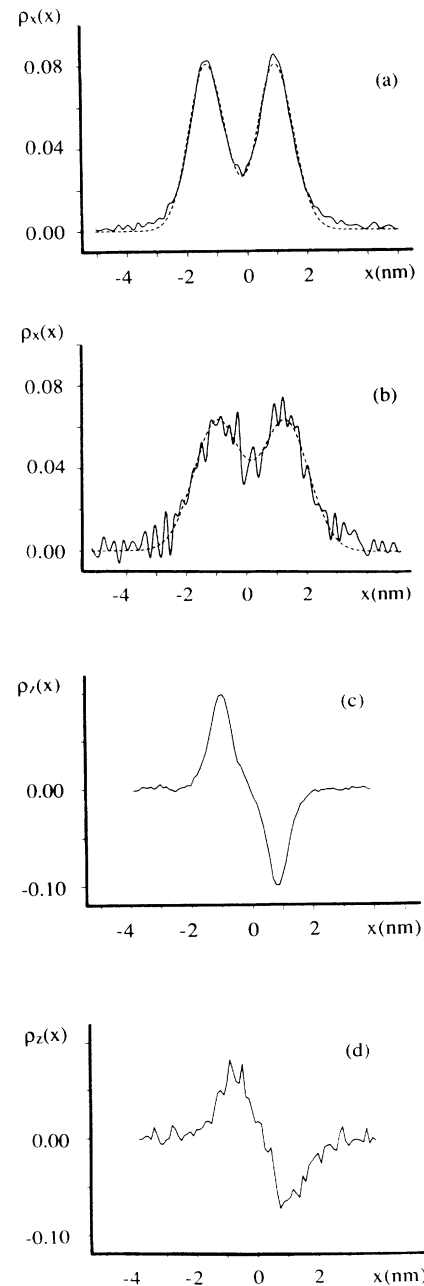

FIG. 4. Burgers vector density distributions at $T=107$ K [(a) and (c)] and $T=1309$ K [(b) and (d)]. (a) and (b) edge components, $\rho_x(x)$, (c) and (d) screw components $\rho_z(x)$. The fault ribbon is entirely invaded by the relaxed cores of the partial dislocations. Solid lines correspond to MD results and dashed lines in (a) and (b) to the fit by two Gaussians shifted with respect one to another by r_0, the dissocation distance.
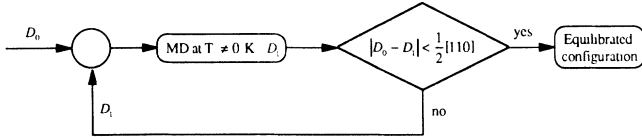
FIG. 5. Schematic illustration of the procedure used to set up the system at each temperature. Convergence is assumed to occur when the separation of the partial dislocations remains stable within a [110] coincidence distance.

long enough to stabilize the partial dislocations at their new equilibrium distance. This iterative scheme was repeated until the final separation between the partial dislocations becomes practically identical to the input value.

Finally, the influence of the static boundaries on the dynamical behavior of atoms pertaining to the inner region provided a criterion upon the adequency of the linear dimensions chosen for our mode. From Fig. 2 it can be seen that the values of the maxima of local-density profiles near the static walls differ from those in the bulk of the dynamical region. However, the perturbation extends only over about 4 Å, near the boundaries and therefore it should not affect our results because of the overall spatial extension of the dynamical region $L \approx 103$ Å.

Despite all these precautions one may doubt on whether or not the partial dislocations are in an unconstrained equilibrium position. We therefore studied, for reference purposes, a system consisting in $N = 11\,328$ point particles and containing a tilt $\theta = 5°84$ sub-boundary made up of perfect $\frac{1}{2}[110](\bar{1}11)$ dislocations. Full periodic-boundary conditions were applied to the system which impose the presence of a mirror image sub-boundary into the system. For this reason we adopted linear dimensions large enough, approximately equal to those of a perfect crystal: $118 \times ([110]) \times 4 ([1\bar{1}2]) \times 2([1\bar{1}1])$ to avoid undesirable interaction effects between the two boundaries. By relaxing or heating up this system the dislocations spontaneously dissociate and finally adopt their equilibrium separation. For low misorientations the dissociation distance is not affected from the fact that the dislocations are organized in a boundary.[30] The dissociation distance we determined equals the value of the separation distance between the partial dislocations we found for the model in the center of the present study (cf. Sec. II C) and thus establishes that the precautions taken during the system preparation are sufficient.

III. RESULTS

A. Core structure

By comparing the local-density distributions shown in Fig. 2 for two different temperatures, one can qualitatively deduce that the core of the partial dislocations is not localized and that their extension increases at increasing temperature. This is more precisely quantified by examining the evolution of the Burgers vector density distributions, $\rho_x(x)$ [Figs. 4(a) and 4(b)] and $\rho_z(x)$ [Figs. 4(c) and 4(d)] as a function of temperature. The fault ribbon is entirely invaded by the anelastic displacements associated

with the cores even at low temperature. This feature becomes more pronounced at high temperature as can be seen by comparing Figs. 4(a) and 4(b). The fault ribbon structure is therefore different from that of a perfect stacking fault and deviates increasingly from it on increasing the temperature.

The area under the two Gaussians fitting the dislocation density profile, is temperature independent, as expected, since it represents the total Burgers vector which is of course conserved. This result gives confidence to the fitting procedure and also indicates that the size of the system is large enough to minimize the influence of the boundary conditions on the core properties.

An alternative method to investigate the core structure is provided by calculating the spherical pair distribution function $g(r)$ on a local basis. This is obtained (Sec. II E) by forcing at least one of the atoms of the considered atom pairs to lie within a narrow cylinder, the pipe, surrounding the dislocation lines. The pipe radius equals the half-width of the density distribution of Burgers vectors deduced from Fig. 4. The results shown in Fig. 6 represent time averages over 2000 time steps and allow for a comparison between local distribution functions at $T = 100$ and $T = 1200$ K as well as with the perfect crystal at $T = 100$ K. At the highest temperature (dashed line) the local distribution function displays liquidlike features since many of the crystalline structure peaks are absent. This bears witness of the existence of premelting effects in the dislocation cores and raises the question of whether or not the liquid germinates therein below the bulk melting temperature. This result is somewhat similar to those obtained by MD simulations of the high-temperature structure in high-angle-tilt grain boundaries[31] for which it has been firmly established, both experimentally[32] and by MD,[33] that although disordered they remain crystalline up to a temperature very close to the melting point. To clarify this point we computed the static structure-factor component $S(k)$ in the pipe as a function of the temperature with $k = (2\pi/a)[\bar{1}11]$. As can be seen from Fig. 7 the $S(k)$ value remains solidlike up to the highest temperature we studied thus suggesting the same conclusion to be valid as the one drawn in the case of grain boundaries. Indeed, the core region is not only statically disordered but in addition, at high temperature, the atoms in the pipe exhibit high vibrational am-
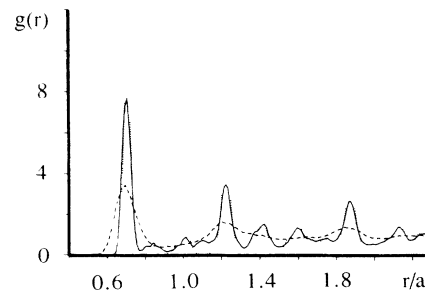

FIG. 6. Radial distribution function $g(r)$ computed in the pipes. Solid line, $T = 100$ K; dashed line, $T = 1200$ K; dotted line, perfect crystal at $T = 100$ K. Thermal averages are performed over 2000 time steps.
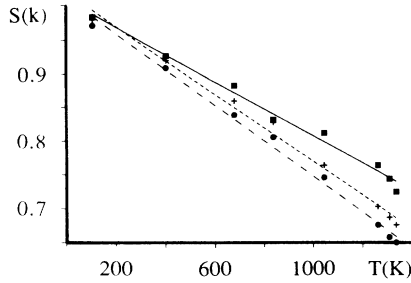
FIG. 7. Local structure factor $S(k)$ component $k=(2\pi/a)[\bar{1}11]$ computed as a function of temperature, in the dislocation core (solid circles). Crosses represent the value $S(k)$ would have, if only Debye-Waller effects were present and squares are the values for the perfect crystal, displayed for reference purposes.

plitudes which contribute to the vanishing of the peaks of $g(r)$ through enhanced Debye-Waller effects. This is illustrated by Fig. 8(a) which displays profiles of atomic MSD along the direction [110] for atoms pertaining to the two $(\bar{1}11)$ atomic planes in the immediate vicinity of the glide plane at different temperatures. Figure 8(b) attests that MSD in the pipes, averaged over the three
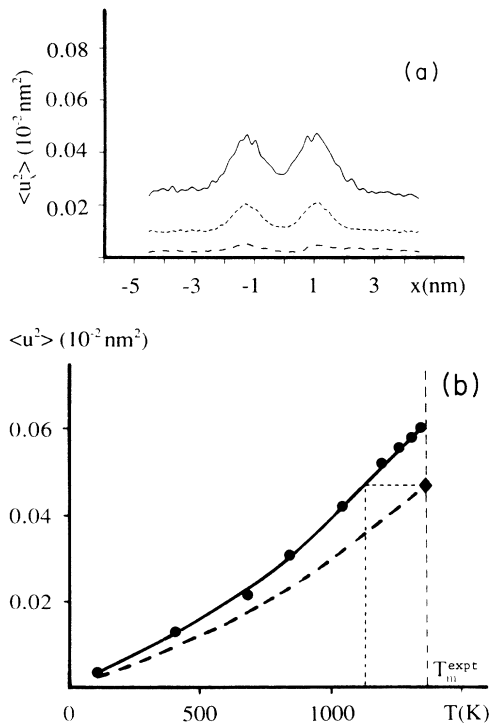

FIG. 8. (a) Atomic mean-square-displacement profiles along the [110] direction at different temperatures. The peaks identify the position of the partial dislocations. Dashed-dotted line, $T = 107$ K; dashed line, $T = 400$ K; solid line, $T = 840$ K; dotted line, $T = 1309$ K. (b) Isotropic atomic mean-square displacements $\langle u^2 \rangle$ in the core region as a function of temperature (solid circles). The dashed line is given for comparison purposes and corresponds to the values obtained for the perfect crystal (Fig. 1). The bulk value at the melting point (diamond) is reached in the pipes at $T \approx 1125$ K.

space directions, rise more rapidly than in the bulk. The bulk value at T_m is indeed reached at $T \approx 0.83 T_m$ inside the pipes. Using the MSD values obtained in the dislocation cores of the Debye-Waller attenuation of $S(k)$ has been computed and is also reported in Fig. 7 as well as the value obtained for the perfect crystal. By comparing these curves and since we carefully verified that in our system point defects are not spontaneously created, we deduce that thermal attenuation effects are mainly at the origin of the above reported results.

B. Dissociation distance and stacking-fault energy

At each temperature the equilibrium dissociation distance can be easily deduced from the Burgers vector density distributions as these given in Fig. 4. Its value is practically temperature dependent, $r_0 \approx 23$ Å, and is comparable with the lower limit of available experimental results.[34,35] However, no special attention should be given to this apparent agreement being this result related to the specific choice we made for the potential cutoff radius $(r_c = 2.3a, \gamma = 73$ mJ/m^2, see Sec. II A).

An estimation of the ribbon fault energy can be easily obtained using the density distributions of Burgers vectors we determined in the framework of the linear, isotropic elasticity approximation:[5,36]

$$\gamma = \gamma_e + \gamma_s \, , \tag{14a}$$

$$\gamma_e = \frac{\mu}{2\pi(1-\nu)} \sum_{i,j} \frac{\rho_{1x}(x_i)\rho_{2x}(x_j)}{x_j - x_i} \Delta x_i \, \Delta x_j \, , \tag{14b}$$

$$\gamma_s = \frac{\mu}{2\pi} \sum_{i,j} \frac{\rho_{1x}(x_i)\rho_{2z}(x_j)}{x_j - x_i} \Delta x_i \, \Delta x_j \, , \tag{14c}$$

where μ is the shear modulus the value of which at each temperature has been fixed to the experimental one,[23] $\rho_{1x}(x_i)$, $\rho_{2x}(x_j)$, $\rho_{1z}(x_i)$, and $\rho_{2z}(x_j)$ the density distributions of Burgers vectors in the core of the partials for the edge and screw components and ν the Poisson modulus. On the other hand, γ_e and γ_s are the respective contributions to the fault ribbon energy of the edge and screw components of the partial dislocations and the value $\nu=0.25$, universal for pair potentials, has been used. The temperature dependence of the ribbon fault energy is, as expected, entirely due to the elastic-shear modulus variation, $\mu=\mu(T)$, as can also be seen by plotting the normalized quantity $F=\gamma\mu(T=0$ K$)/\mu(T)$ versus the temperature (Fig. 9).

The value of the fault ribbon energy at $T=0$ K, deduced from Eqs. (14), $\gamma'=122$ erg/cm^2, turns out to be larger than that of an infinite extension perfect stacking fault at the same temperature, $\gamma=73$ erg/cm^2 (Table II). This difference should be attributed to the extension of the cores, visible in Figs. 2 and 4, and is not surprising since the atomic structure of the fault ribbon differs significantly from that of the perfect stacking fault.

In order to ascertain that the fixed boundary conditions we used do not maintain an artificial constraint on the partial dislocations which may affect the results we also studied the low angle, $\theta=5°84$ tilt sub-boundary made up by introducing in a three periodic system the
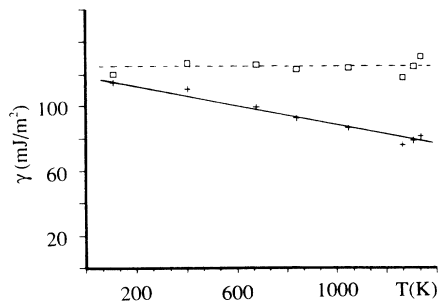
FIG. 9. Stacking-fault energy γ vs temperature (crosses). Open squares represent the temperature dependence of $F = \gamma\mu(T=0)/\mu(T)$; the fault ribbon was energy corrected to remove the elastic-shear-modulus variation. Solid and dashed lines are linear best fits to the data.

adequate number of perfect $\frac{1}{2}a[110](\bar{1}11)$ dislocations (Sec. II F). In this case the dissociation distance of the individual dislocations in the boundary remains unaffected[30] and a comparison can be made with the above reported results. Figure 10 displays a typical atomic density profile realized by adding local densities taken in the vicinity of the slip plane of one of the sub-boundary dislocations. These dissociate spontaneously and when the system is equilibrated lead to the same dissociation distance as that we found for the isolated dislocation.

C. Melting

As has been reported above, despite the existence of premelting phenomena in the core region no local melting has been found to occur in it. This however does not imply that local melting should not take place. Indeed, in addition to metastability effects which may immoderately delay such a phenomenon to occur on the time scale typical of MD calculations (≤ 1 ns), the large fluctuations existing in small systems, such as the one we employed in present study, do not allow us to fix the temper-
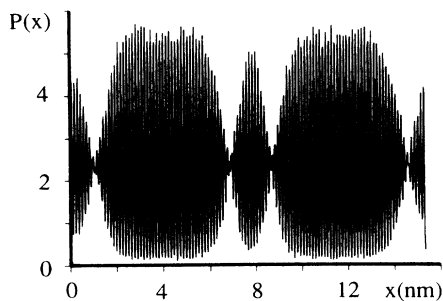
ature at a value arbitrarily close to the bulk melting point. Therefore, local melting cannot be studied using MD. Instead, one can ask the question on whether or not the nucleation barrier of the liquid is lower in the vicinity of the dislocation lines than in the bulk. We tried to qualitatively address this question by observing the melting of the system settled up in a superheated state as follows: starting from an initial equilibrium configuration at $T = 1337$ K, the atomic velocities are increased every 200 time steps by a multiplicative factor until the total energy of the system becomes high enough to initiate melting. Among the resulting configurations a few only have melted during an additional trajectory lasting $10^4 - 2 \times 10^4$ time steps. The observed behavior in those cases displays the common feature that melting is systematically initiated in the vicinity of the dislocation cores and of the fault ribbon. This is, qualitatively illustrated by the series of trajectory plots at $T = 1605$ K, shown in Fig. 11, each of which represents the atomic trajectories in the plane immediately below the glide plane during 10^3 time steps. Melting starts in the defective region and propagates into the bulk. Our results suggest that the nucleation barrier for the liquid is smaller near the dislocation cores and the fault ribbon than in the bulk, although statistics need to be improved in order to ascertain this qualitative conclusion (only three different superheated configurations among those produced led to melting). Moreover, the lowest temperature for which melting has been observed to occur, $T = 1605$ K, provides an upper limit for the melting point of our system ($T_m^{exp} \approx 1356$ K).

P(x)

FIG. 10. Local-density-profile along [110] in a system containing a $\theta = 5°84$ tilt boundary. The boundary consists in a pileup of $\frac{1}{2}[110](\bar{1}11)$ dislocations which split spontaneously into Shockley partial dislocations. A second image boundary is introduced by the periodic limit conditions. The figure is obtained by subtracting the local-density profiles computed for the two ($\bar{1}11$) planes surrounding the glide plane. The dissociation distance computed in this system equals that of the isolated dislocation we studied.
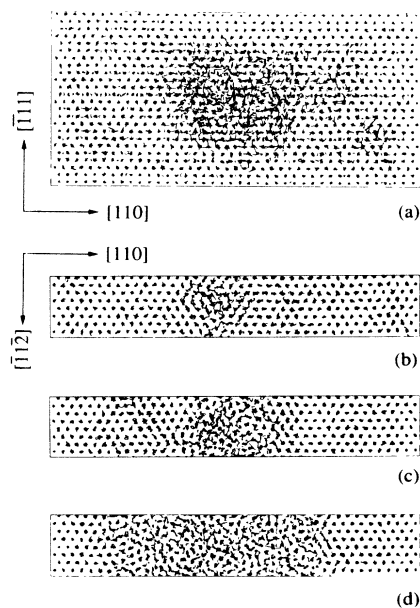
FIG. 11. Trajectories of atoms belonging to the plane immediately below the slip at $T = 1605$ K. The disordered region indicates enhanced diffusion corresponding to the nucleation of the liquid. (a) Trajectories of the system recorded during 5000 time steps and projected onto a ($1\bar{1}2$) atomic plane. (b), (c), and (d) growth of the liquid nucleus; trajectories are recorded during 1000 time steps starting at 2000, 7000, and 14000 time steps, respectively, and are projected onto a ($\bar{1}11$) atomic plane.

IV. DISCUSSION AND CONCLUSIONS

The central result of the present study sheds light on the increasing extension of the cores of Shockley partial dislocations when the temperature increases while their separation distance remains constant. A natural consequence of this behavior is the resulting variation of the atomic structure of the fault ribbon and of its energy with respect to that of a perfect stacking fault. Although old[24] and also recent studies[37] have suggested the existence of such effects and examined the possible causes, this is the first time at which the role of the core structure is undoubtedly identified at the atomic scale. Our study, though willingly devoted to a model system which mimics real copper, should be essentially considered from a generic point of view and thus we believe our results to be applicable to a wide class of fcc structure metals. An important question which unavoidably arises concerns the meaning of experimental determinations of the stacking-fault energy by electron microscopy measurements of the dissociation distance between partial dislocations. Indeed, our study strongly suggests that these should be seriously questioned when the dissociation distance is comparable to the length scale of the cores extension.

As we already mentioned, in metals with the hexagonal structure the extended cores model explains exhaustively the variety of easy-glide planes, basal or prismatic, observed experimentally.[4] On the other hand, recent experimental investigations of the anomalous elastic limit in beryllium attributed this phenomenon to a possible intrinsic (not shear modulus dependent) variation of the stacking-fault energy.[37] Based on the results of the present study, work in progress is devoted to the study of the core structure of dislocations in beryllium, of its temperature dependence, and its relation with the elastic limit of this material.

In conclusion, we investigated the temperature dependence of the core structure of the Shockley partial dislocations resulting from the dissociation of a perfect, easy-glide dislocation in copper. Our results show that the cores of the partial dislocations become increasingly extended at increasing the temperature while the dissociation distance remains constant. This effect leads to a progressive change in the structure of the fault ribbon which, therefore, fundamentally differs from the perfect stacking fault of infinite extension. In the framework of linear, isotropic elastic theory of dislocations our results indicate that the energy of the fault ribbon decreases on increasing temperature, yet this behavior is entirely due to the elastic shear modulus decrease. Moreover, at high temperatures the atomic structure inside the pipes is highly disordered but no point defects were observed to nucleate spontaneously. The disorder is related to amplitudes of atomic vibrations in the cores which are much larger than those of bulk atoms. Finally, we observed that in the superheated state, melting is initiated in this system systematically in the region near the cores and the fault ribbon. Thus, we concluded in favor of a nucleation barrier for the liquid being lower near the defect than in the bulk. Our study of dislocation initiating melting concerned only the qualitative aspects of this phenomenon.

Therefore, we have not attempted to develop a comparison with existing work devoted to a quantitative investigation of how melting occurs in presence of defects. It should be mentioned however that similar to dislocations grain boundaries are preferential sites for the nucleation of the liquid. This is the conclusion of recent MD simulations of melting in silicon and copper bicrystals.[38,39]

APPENDIX

The dislocation core structure may be conveniently described by a density distribution of infinitesimal dislocations, which is given by the spatial derivatives of the disregistry in the direction [110] parallel to the Burgers vector:[36]

$$\rho_x(x_i) = \frac{\Delta}{\Delta x_i}[\delta u_x(x_i)] \ , \tag{A1a}$$

$$\rho_z(x_i) = \frac{\Delta}{\Delta x_i}[\delta u_z(x_i)] \ , \tag{A1b}$$

where $u_i(x)$ represent the $i = x,z$ components of relative displacements above and below the glide plane along the [110] and [1$\bar{1}$2] directions, and $\rho_x(x),\rho_z(x)$ verify the following conditions:

$$\sum_{i=-\infty}^{+\infty} \rho_x(x_i)\Delta x_i = b \ , \tag{A2a}$$

$$\sum_{i=-\infty}^{+\infty} \rho_z(x_i)\Delta x_i = 0 \ , \tag{A2b}$$

expressing the conservation of the Burgers vector.

From Eq. (A1a) we deduce the relationship between the distribution density, say $\rho_x(x)$, and the local deformations

$$\rho_x(x_i) = \frac{\Delta}{\Delta x_i}[u_x^l(x_i) - u_x^h(x_i)]$$

$$= \varepsilon_{xx}^l - \varepsilon_{xx}^h = \frac{d^l - d_0}{d_0} - \frac{d^h - d_0}{d_0} = \frac{d^l - d^h}{d_0} \ , \tag{A3}$$

where the indexes h (high) and l (low) stand for quantities computed above and below the glide plane and d^l, d_0, represent the spacing of [1$\bar{1}$2] atomic columns in the dislocated and in the perfect lattice, respectively. A similar expression holds for $\rho_z(x)$. The determination of average values for d^l, d_0, allows us to plot the curves displayed in Fig. 4.

*To whom correspondence should be addressed.

[1] R. E. Peierls, Proc. Phys. Soc. London **52**, 34 (1940).

[2] F. R. N. Nabarro, Proc. Phys. Soc. London **59**, 256 (1947).

[3] D. J. Bacon and J. W. Martin, (a) Philos. Mag. A **43**, 883 (1981); (b) *ibid.* A **43**, 901 (1981).

[4] B. Legrand, in *Dislocations 1984, Comptes Rendus du Colloque International du C.N.R.S. Dislocations: Structure de Coeur et Propriétés Physiques,* edited by P. Veyssière, P. Kubin, and J. Castaing (Editions du CNRS, Aussois, France, 1984), p. 73.

[5] J. P. Hirth and J. Lothe, *Theory of Dislocations* (Wiley, New York, 1982).

[6] V. Vitek, Scr. Metall. **9**, 611 (1975).

[7] M. Wuttig and K. H. Birnbaum, Phys. Rev. **147**, 495 (1966).

[8] R. W. Baluffi and A. V. Granato, in *Dislocations in Solids,* edited by F. R. N. Nabarro (North-Holland, Amsterdam, 1979), Vol. 4, p. 1.

[9] J. Huang, M. Meyer, and V. Pontikis, Phys. Rev. Lett. **63**, 628 (1989).

[10] J. Huang, M. Meyer, and V. Pontikis, Philos. Mag. (to be published).

[11] L. Dagens, J. Phys. F **7**, 1167 (1977).

[12] N. Q. Lam, L. Dagens, and N. V. Doan, J. Phys. F **11**, 793 (1981).

[13] P. G. Gehlen, Rev. Sci. Instrum. **40**, 715 (1969).

[14] L. Dagens (private communication).

[15] M. S. Duesbery, G. Jacucci, and R. Taylor, J. Phys. F **9**, 413 (1979).

[16] J. Huang, M. Meyer, and V. Pontikis, Scr. Metall. **22**, 463 (1988).

[17] J. C. Updahyaya and L. Dagens, J. Phys. F **8**, L21 (1978); **9**, 2177 (1979).

[18] (a) E. A. Owen and R. W. Williams, Proc. R. Soc. London, Ser. A **188**, 509 (1947); (b) P. A. Flinn, G. M. McManus, and J. A. Rayne, Phys. Rev. **123**, 809 (1961).

[19] C. J. Martin and D. A. O'Connor, Acta Crystallogr. Sect. A **34**, 500 (1978).

[20] V. Rosato, M. Guillopé, and B. Legrand, Philos. Mag. A **59**, 321 (1989).

[21] F. A. Lindemann, Phys. Z. **11**, 609 (1910).

[22] J. J. Gilvarry, Phys. Rev. **102**, 308 (1956).

[23] W. C. Overton and J. Gaffney, Phys. Rev. **98**, 969 (1955).

[24] P. C. J. Gallagher, Metall. Trans. **1**, 2429 (1970).

[25] L. Verlet, Phys. Rev. **159**, 981 (1967).

[26] C. Bennett, in *Diffusion in Solids-Recent Developments,* edited by A. S. Nowick and J. J. Burton (Academic, New York, 1975), p. 73.

[27] J. Huang, Ph.D. thesis, Université Paris VI, 1989, unpublished.

[28] G. Ciccotti, M. Guillope, and V. Pontikis, Phys. Rev. B **27**, 5576 (1983).

[29] R. C. Perrin, A. Englert, and R. Bullough, in *Interatomic Potentials and Simulation of Lattice Defects,* edited by P. C. Gehlen, J. R. Beeler, Jr., and R. I. Jaffee (Plenum, New York, 1972), p. 525.

[30] Y. Minonishi and R. Horiuchi, J. Phys. (Paris) Colloq. **49**, C5-461 (1988).

[31] V. Rosato, G. Ciccotti, and V. Pontikis, Phys. Rev. B **33**, 1860 (1986).

[32] Siu-Wai Chan, J. S. Liu, and R. W. Balluffi, Scr. Metall. **19**, 1251 (1985).

[33] V. Pontikis, J. Phys. (Paris) Colloq. **49**, C5-32 (1988).

[34] D. J. H. Cockayne, M. L. Jenkins, and I. L. F. Ray, Philos. Mag. **24**, 1383 (1971).

[35] W. M. Stobbs and G. H. Sworn, Philos. Mag. **24**, 1365 (1971).

[36] D. J. H. Cockayne and V. Vitek, Phys. Status Solidi B **65**, 751 (1974).

[37] A. Couret and D. Caillard, Philos. Mag. A **59**, 783 (1989); (b) A **59**, 783 (1989).

[38] S. R. Phillpot, J. F. Lutsko, D. Wolf, and S. Yip, Phys. Rev. B **40**, 2831 (1989).

[39] J. F. Lutsko, D. Wolf, S. R. Phillpot, and S. Yip, Phys. Rev. B **40**, 2841 (1989).